SSRG International Journal of Electrical and Electronics Engineering
ISSN: 2348-8379/ https://doi.org/10.14445/23488379/IJEEE-V11I7P106

Volume 11 Issue 7, 66-77, July 2024

Original Article

Enhancing Independent Microgrid Frequency Control with PV-HESS System: Integration of Virtual Synchronous Generator Controller

Hung Nguyen-Van[1,2*], Hoan Hoang-Van[2], Huy Nguyen-Duc[1]

[1]*Hanoi University of Science and Technology, Hanoi, Vietnam.*
[2]*Hanoi University of Industry, Hanoi, Vietnam.*

[*]*Corresponding Author : hung_nv@haui.edu.vn*

Received: 03 May 2024 Revised: 05 June 2024 Accepted: 03 July 2024 Published: 26 July 2024

Abstract - *The autonomous operation of photovoltaic-based microgrids is strongly reliant on the integration of energy storage systems, notably Hybrid Energy Storage Systems (HESS) that include super capacitors. However, the lack of rotational inertia in PV-HESS power systems can cause undesirable frequency oscillations in reaction to changes in load demand or rapid swings in irradiance levels. This paper presents a control paradigm for PV-HESS systems based on a Virtual Synchronous Generator (VSG) controller. VSG controllers aid in increasing system inertia and facilitating frequency regulation in microgrids. Simulations were run on the Matlab/Simulink platform with varied load circumstances and irradiance levels.*

Keywords - *Microgrid, PV, HESS, VSG, Lack of inertia.*

1. Introduction

The creation of a microgrid by combining renewable energy sources with local loads is crucial for enhancing power supply dependability and optimizing the potential of decentralized sources [1]. Photovoltaic systems are commonly employed among renewable energy sources due to several benefits, but it is important to consider the unpredictable nature of solar energy when integrating solar power systems into small-scale grids that are susceptible to power source fluctuations, particularly in off-grid scenarios [2]. A HESS is viewed as an efficient remedy for addressing the challenges arising from the intermittent nature of PV power. This solution contributes to enhancing the dependability and quality of electricity in small grids. By integrating various storage technologies, including battery systems and super capacitors, HESS can offer substantial storage capacity while swiftly adapting to fluctuations in power supply [3, 4].

However, microgrids operating based on HESS-integrated PV systems still encounter a major problem, which is the lack of inertia [5]. Traditional power systems rely on the rotational inertia of synchronous generators to maintain grid stability. The rotational inertia stored in synchronous generator rotors mitigates agitation during load changes as well as when generators suddenly change output due to energy changes in the primary sources. The HESS hybrid PV system lacks this mechanical inertia [6, 7].

In prior research, VSGs have been advanced as a solution to compensate for the absence of rotational inertia in power systems. These controllers emulate the inertia and dynamic behavior of conventional synchronous generators, thus proving instrumental in stabilizing both frequency and voltage levels. The mechanism of inertia compensation in smaller power grids involves the utilization of power converters that mimic the operational dynamics of synchronous generators. Configurations for simulating virtual inertia can generally be categorized into three types: those based on the synchronous generator model, those derived from rotational equations, and those dependent on power-frequency response characteristics [8].

The synchronous generator-based simulation configuration is constructed on the comprehensive dynamic model of a Synchronous Generator (SG), encompassing both its electrical and mechanical components. This thorough emulation of SG dynamics enhances the accuracy of the configuration, as noted in the literature [9]. In contrast, Ise Lab [10, 11] introduced a configuration centered solely on the rotational equation, aiming to simulate virtual inertia by replicating the rotational dynamics of the SG. This approach specifically measures grid frequency and the active power output of the converter. Furthermore, VSYNC [12] developed a virtual inertial simulation configuration that relies on power-frequency response. This method utilizes variable frequency differential measurement parameters to execute virtual

observation simulations, emphasizing dynamic response over static state replication. Significantly, much of the research in microgrid voltage and frequency control has concentrated on configurations based on rotational equations. This preference is attributed to their practical applicability and relatively moderate complexity, making them particularly suited for real-world implementations where the balance between fidelity and operational simplicity is crucial.

Multiple research has suggested implementing control of ESS using the VSG architecture [13]. These investigations constantly confirm that ESS plays a vital role in improving the stability of microgrids, which have little inertia and are vulnerable to power fluctuations. Furthermore, this research has proposed specific arrangements for implementing the VSG model to regulate conventional ESS. Nevertheless, there has been limited research on the utilization of HESS, specifically those that integrate super capacitors, in the existing literature. This is particularly relevant in the context of DC power systems that have primary sources, such as PV solar power systems.

Implementing the VSG controller within a PV-HESS in microgrids necessitates careful consideration of grid frequency sensitivity to factors such as stochastic variations in solar irradiance and the charge-discharge dynamics of energy storage components. The HESS encompasses the coordinated charging and discharging of batteries and super capacitors alongside load-shifting strategies. Fluctuations in solar radiation necessitate adaptive adjustments in the HESS's charging and discharging protocols to ensure that the output power from PV-HESS aligns with the variable demands of electrical loads, particularly under unpredictable operational conditions. These considerations are essential for the successful application of a VSG controller to a PV-HESS in ensuring stable microgrid operation. This article details the development of a VSG controller modeled on an island-mode Microgrid, utilizing a modified IEEE 6 Bus grid model [14].

This modified grid model incorporates multiple photovoltaic sources and simulates various scenarios of changing radiation intensity and fluctuating electrical loads as per a predefined load map. The simulation and evaluation of these scenarios are conducted using the Matlab/Simulink software, facilitating detailed analysis of the VSG controller's performance under diverse and dynamic conditions. This methodological approach underscores the importance of integrating advanced simulation tools to enhance the resilience and reliability of microgrid energy systems.

2. Virtual Synchronous Generator Model of PV–HESS

The PV-HESS system demonstrates significant operational flexibility, allowing it to switch between directly providing power to loads and storing energy for later use during periods of solar irradiation. Moreover, this system excels at managing high-capacity charging and discharging in brief time periods, a critical capability for addressing sudden power swings. This capacity is made possible by the integration of a hybrid storage system that combines conventional energy storage with super capacitors.

Integrating the VSG simulation model into the PV-HESS system is crucial for tackling the issue of reduced rotational inertia in microgrids. By utilizing a VSG controller, the system is able to replicate the inertia properties of conventional synchronous generators, hence improving the stability and resilience of the power supply. The efficacy of this method is demonstrated in the suggested VSG model shown in Figure 1.

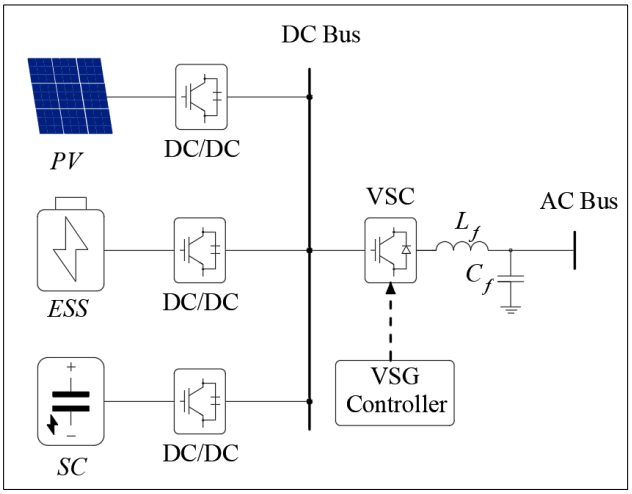

Fig. 1 Virtual synchronous generator simulation model of PV-HESS

This concept not only addresses the natural absence of physical inertia but also enhances the resilience and adaptability of energy management strategies in microgrid contexts. The progress in VSG technology is crucial for enhancing the integration and efficiency of renewable energy sources in contemporary power systems.

The hybrid power model integrates PV panels with a HESS that includes both ESS and super capacitors. In this design, the PV array and the HESS are connected in parallel using a DC link. Furthermore, the model is specifically designed to actively supply power to the load, mostly using the electricity generated by the PV panels during periods of solar radiation. The HESS plays a crucial role in mitigating power disruptions [15].

2.1. Modeling PV Photovoltaic Cells

The model includes a current source that is coupled in parallel with a diode. It incorporates essential parameters to simulate the fundamental characteristics of PV panels, such as the short-circuit current ISC and the open-circuit voltage VOC. In order to improve the precision of the model, a resistor

RS is connected in series, and a resistor RP is connected in parallel. Figure 2 depicts this simplified model [16].

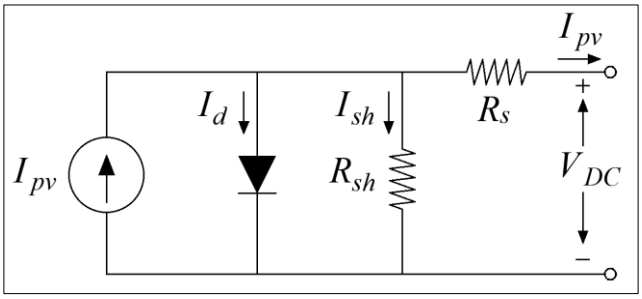

Fig. 2 PV circuit model

The mathematical model of the PV module is calculated through the equation:

$$I = I_{PV} - I_0\left[e^{\frac{q(V+IR_S)}{akT}} - 1\right] - \left[\frac{V+IR_S}{R_P}\right] \quad (1)$$

In there,
I_{PV} : The photoelectric current (A)
I_0 : The saturation current of the diode (A)
q : 1,602×10-19 C
K : 1, 38×10-23 J/K
a : The ideal coefficient of the diode
R_S : The series resistance (Ω)
R_P : The parallel resistance (Ω)
T : The temperature in Kelvin (K)

I_{PV} is a function of irradiance (G) and is expressed as:

$$I_{PV} = \left[I_{PV\_STC} + K_i\Delta T\right]\frac{G}{G_{STC}} \quad (2)$$

In there,
I_{PV_STC} : The current emitted with light under Standard Conditions (STC)
ΔT = T = TSTC (K)
G : Cell surface radiation (W/m^2)
GSTC : 1000W/m^2 is radiation according to STC
K_i : The short-circuit current coefficient

The diode saturation current (I_0) is given as:

$$I_0 = I_{0\_STC}\left(\frac{T}{T_{STC}}\right)^3 \exp\left[\frac{qE_g}{ak}\left(\frac{1}{T_{STC}} - \frac{1}{T}\right)\right] \quad (3)$$

In there,
I_{0STC} is the saturation current under STC
T_{STC} is the temperature under STC

The P&O algorithm is used to maximize the output power of the PV module by determining the operating point on the characteristic curve that results in the highest power output, which is referred to as the maximum power point.

2.2. HESS Modeling

The HESS model outlined in this study consists of a BESS and a super capacitor model, both coupled in parallel and equipped with a bidirectional DC/DC converter. These converters aid in voltage conversion and ensure a consistent output voltage at the DC link. Bidirectional DC/DC converters are included in the HESS, allowing for flexible regulation of power generation capacity and the conversion of excess power into stored energy. This feature highlights the system's ability to control the movement of energy inside the microgrid effectively.

2.2.1. BESS Modeling

The mathematical model used to replace the BESS utilizes Lithium-ion battery technology and represents the operation of the BESS through the State of Charge-discharge (SOC). The SOC, as defined in reference [17].

An alternative circuit model representing a BESS using Lithium - Ion battery technology is shown in Figure 3 [18]:

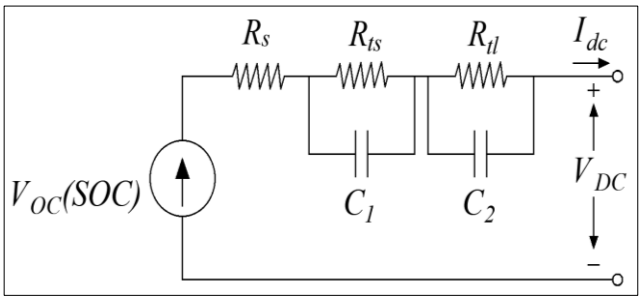

Fig. 3 Circuit model of BESS

The circuit comprises an open circuit voltage V_{DC} and three series resistors (R_s, R_{ts}, R_{tl}) that represent distinct electrochemical processes. The open circuit voltage and three resistors exhibit nonlinearity with respect to the State of Charge (SOC) and can be mathematically represented as follows:

$$\begin{cases} V_{oc} = a_0 e^{(-a_1 SOC)} + a_2 + a_3 SOC - a_4 SOC^2 + a_5 SOC^3 \\ R_s = b_0 e^{(-b_1 SOC)} + b_2 + b_3 SOC - b_4 SOC^2 + b_5 SOC^3 \\ R_{ts} = c_0 e^{(-c_1 SOC)} + c_2 \\ R_{tl} = d_0 e^{(-d_1 SOC)} + d_2 \\ R_{tot} = R_s + R_{ts} + R_{tl} \end{cases} \quad (4)$$

The current in the circuit can be obtained by solving the quadratic equation $P_e = I.(V_{oc} - R_{tot}.I)$:

$$I = \frac{V_{oc} - \sqrt{V_{oc}^2 - 4.R_{tot}.P_e}}{2.R_{tot}} \quad (5)$$

The charging and discharging efficiency of the BESS is given by:

$$\begin{cases} \eta^{ch} = \dfrac{V_{oc}}{V_{oc} - R_{tot}.I} \\ \eta^{dis} = \dfrac{V_{oc} - R_{tot}.I}{V_{oc}} \end{cases} \quad (6)$$

The characteristic curve of the Lithium - Ion battery is described in Figures 4 and 5.

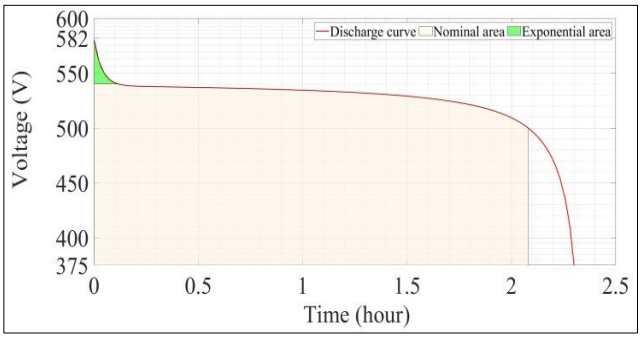

Fig. 4 V-I characteristic curve of the BESS

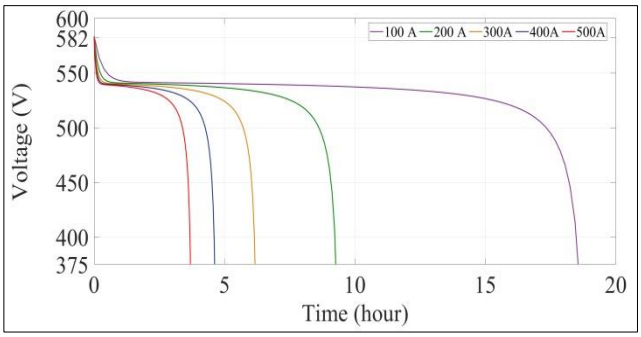

Fig. 5 BESS capacity curve with nominal discharge current

2.2.2. Supercapacitor Modeling

The circuit model used to replace the supercapacitor utilizes identical physical components to replicate its behavior, such as Rp and C0, accurately. In addition, the series resistor and cell resistor are denoted as R_{ESR}. Additional components, such as R_s, R_{ss}, and C_{ss}, are incorporated to define the behavior of the supercapacitor during discharge and transient response. The components are specified in Figure 6. Mathematical modeling provides an accurate representation of the physical structure, chemical interactions, and current distribution within a capacitor. These models utilize mathematical equations to depict the dual modes of charging and discharging that are characteristic of supercapacitors [19].

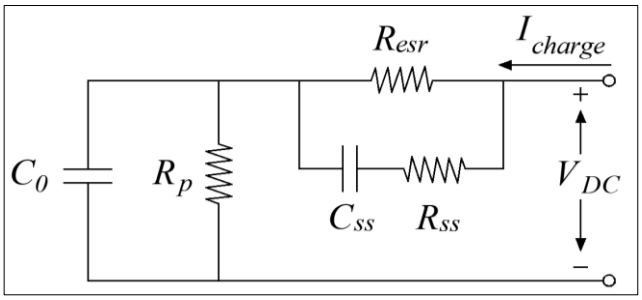

Fig. 6 Circuit model of supercapacitors

$$V_{charge} = I_{charge} \times R_{esr} + I_{charge} \times R_{leak} \times \left(1 - e^{\left(\frac{-t}{R_{leak} \times C_{complet}}\right)}\right) \quad (7)$$

$$V_{discharge} = V_{charge} - I_{discharge} \times R_{esr} - (V_{discharge-1} + I_{discharge} \times R_{leak}) \times \left(1 - e^{\left(\frac{-t}{R_{leak} \times C_{complet}}\right)}\right) \quad (8)$$

with,

$V_{charge}/V_{discharge}$	:	Charge/discharge voltage value (V)
$I_{charge}/I_{discharge}$	:	Charge/discharge current value (A)
R_{ESR}	:	The equivalent series resistance (Ω)
R_{leak}	:	High resistance inside (Ω)
$C_{complet}$	:	The capacitance value (F)
T	:	Time (s)

Numerous factors, such as age, humidity, nominal voltage, and ambient conditions, affect the values of R_{leak}, $C_{complet}$, R_{ESR}, and R. The following formula can be used to get the supercapacitor's capacitance value:

$$C_{complet} = C_0(F) \times C_{cycle-life}(\%) \quad (9)$$

The lifespan of the supercapacitor is presented as follows:

$$C_{cycle-life}(\%) = 100 - \alpha^{\left(\frac{T-T_{ref}}{10}\right)} \times \sqrt{N} \times \left(\frac{V - V_C}{V}\right) \times H \quad (10)$$

In there,

α	:	The acceleration coefficient
T	:	The operating temperature (K)
T_{ref}	:	The reference operating temperature
N	:	The number of cycles used
V	:	The voltage range (V)
V_c	:	The nominal voltage (V)
H	:	Represents the proportion of ambient humidity.

The resistance of a supercapacitor is influenced by its temperature and dimensions. The resistance R_{ESR} of the supercapacitor increases as the temperature lowers. Consequently, the discharge efficiency of the supercapacitor diminishes when it runs at low temperatures. The R_{ESR} equation is constructed in the following manner:

$$R_{ESR} = b_1 \times R_{\mathrm{ESR0}} \times \left(1 + \gamma \times \left(T - T_{ref}\right)\right) + b_2 \times R_{\mathrm{ESR0}} \times e^{\left(\left(\frac{-K_t}{2}\right) \times \left(T - T_{ref}\right)\right)} \quad (11)$$

In which,

T_0 : 293 K

γ = 0.07 K^{-1} : The temperature coefficient of the composite aluminum and carbon components.

kT = 0,045 K^{-1} : The synthetic ion activation energy component.

R_{ESR0} : The theoretical series resistance.

The V–I characteristic curve of the supercapacitor is shown in Figure 7.

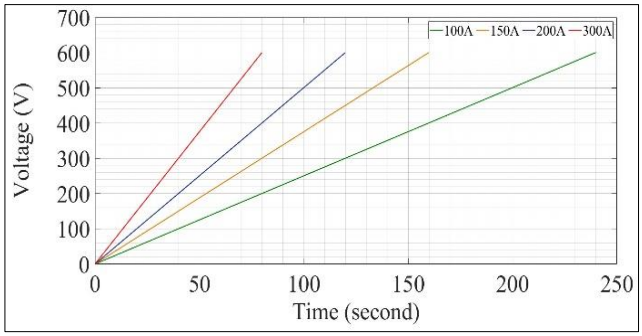

Fig. 7 V-I characteristic curve of supercapacitor

2.2.3. Bidirectional DC-DC Converter Model

The bidirectional DC/DC converter in the HESS is responsible for regulating the voltage and current from the BESS or supercapacitor to align with the reference voltage. This ensures that the DC link remains stable during discharge in DC mode. On the other hand, when the system is being charged, control converters regulate power semiconductor valves to direct the charging current into the HESS system in order to handle any excess capacity. Figure 8 illustrates the arrangement of the power circuit and its controller. During discharge, the circuit functions in two distinct modes: continuous current mode and intermittent mode. During continuous current mode, the inductor retains enough energy to fulfill the load's requirements, ensuring a consistent current flow until the next on/off cycle. This guarantees that the load is provided with a consistent and steady flow of voltage and current. In this operational state, if the output voltage is above the input voltage, the converter will determine the output voltage using the following calculation:

$$V_{out} = \frac{1}{1-k} V_{in} \quad (12)$$

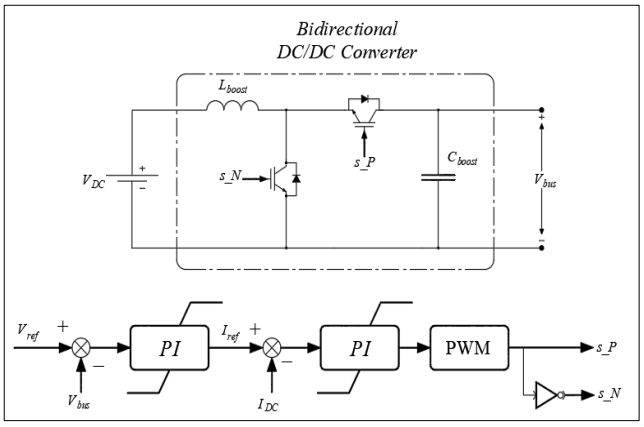

Fig. 8 Bidirectional DC/DC converter model structure and controller

Discontinuous current mode results in an output voltage for the converter:

$$V_{in} kT + \left(V_{in} - V_{out}\right)\Delta_1 T = 0 \quad (13)$$

$$V_{out} = \frac{\Delta_1 + k}{\Delta_1} V_{in} \quad (14)$$

In there:

V_{out} : Output voltage of the converter

V_{in} : Input voltage of the converter

k : Duty cycle

T : Switching time

Δ_I : Period during which the inductor voltage is negative.

A mathematical equation regulates the process of charging and discharging a capacitor:

$$\frac{C}{2}\frac{dv_{dc}{}^2}{dt} = P_{BESS} - P_{AC} \quad (15)$$

$$P_{AC} = v_d i_d + v_q i_q \quad (16)$$

Discharge mode:

$$V_{batt} = E_0 - R.i - K\frac{Q}{Q - it}(it + i^*) + A.e^{(-B.it)} \quad (17)$$

Charging mode:

$$V_{batt} = E_0 - R.i - K\frac{Q}{it-0.1Q}i^* - K\frac{Q}{Q-it}it + e^t \quad (18)$$

2.3. DC/AC Voltage Converter

The microgrid utilizes a PV-HESS power system that operates as a voltage source in autonomous mode. In this mode, the control of frequency and voltage mostly depends on the voltage source converter [20, 21]. This converter functions based on predetermined voltage and frequency standards in order to ensure a consistent and steady voltage and frequency throughout the microgrid. The control strategy for the voltage source converter in isolated mode is depicted by a block diagram obtained from simulations employing rotational equations, as seen in Figure 9.

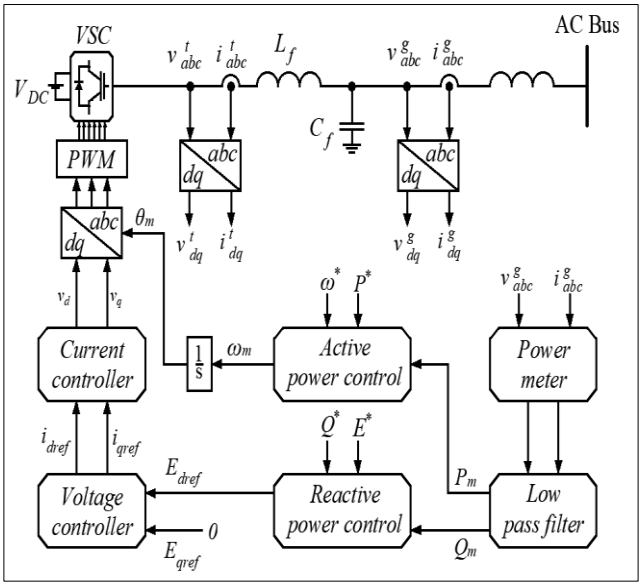

Fig. 9 Block diagram of voltage source power converter control

The control block diagram for the power converter is organized based on essential components, such as "Active Power Control", "Reactive Power Control", "Current Control", and "Voltage Control" blocks. In order to make the control process more efficient, the rotating perpendicular (dq) coordinate system is employed. The conversion of variables from the ABC coordinate axis to the dq rotating coordinate system utilizes the Park transformation formula, enabling efficient control of power dynamics in the system.

Power P, Q in the system of perpendicular axes dq:

$$P_{out} = \frac{\omega_c}{s+\omega_c}(v_d^g.i_d^g + v_q^g.i_q^g) \quad (19)$$

$$Q_{out} = \frac{\omega_c}{s+\omega_c}(v_d^g.i_q^g - v_q^g.i_d^g) \quad (20)$$

2.3.1. Active Power Control Loop

The "Active Power Control" block is divided into two consecutive blocks that reflect the procedures of "Governor" and "Rotational Equation". The "Governor" model, illustrated in Figure 10, is built around the correlation between power P and angular frequency ω, as represented by the distinctive k_p slope relationship. Additionally, it incorporates a delay component defined by a time constant T_d, which replicates the intrinsic mechanical reaction delay of the governor in the SG.

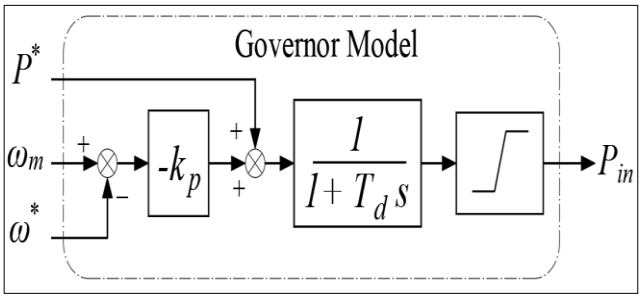

Fig. 10 Speed governor model

$$P_{in} = \frac{1}{1+T_D s}\left(P^* - k_p(\omega_m - \omega^*)\right) \quad (21)$$

Subsequent to the "Governor" model, the "Rotational Equation" model delineates the electromechanical dynamics within the SG, as illustrated in Figure 11. This model provides a detailed representation of the interplay between electrical and mechanical forces operating within the generator.

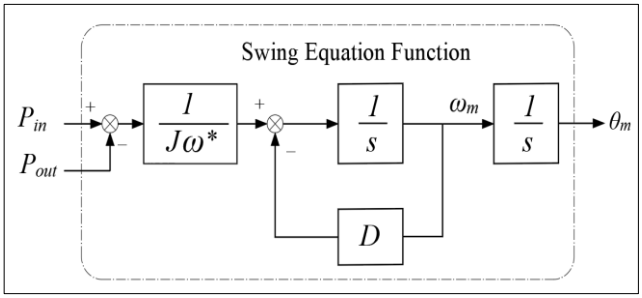

Fig. 11 Rotational equation model

The rotation equation is described as follows,

$$\frac{d\omega_m}{dt} = \frac{1}{J\omega^*}(P_{in} - P_{out}) - D\omega_m \quad (22)$$

$$\frac{d\theta_m}{dt} = \omega_m \quad (23)$$

In there,

J : Rotor moment of inertia (kg.m^2)
ω_m : Angular frequency (rad/s)
D : Damping coefficient (pu)

2.3.2. Reactive Power Control

Concurrently with the frequency control process, which operates through active power management, there is a voltage control process that relies on reactive power (Q) control. The reactive power control process is segmented into two distinct phases, ultimately interfacing with the internal voltage controller of the converter. The Q-V slope control phase, pivotal in this process, is depicted in Figure 12.

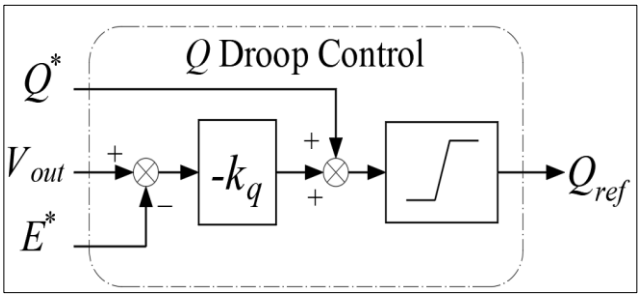

Fig. 12 Reactive power droop control model

A reactive power PI controller is used in conjunction with the reactive power droop controller to replicate the functionality of the Automatic Reactive power controller (AQR) in the SG. The PI controller is illustrated in Figure 13.

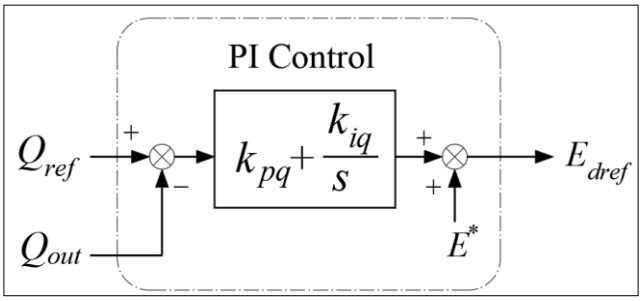

Fig. 13 Reactive power PI controller

In there,

$$Q_{ref} = Q_o - k_q(V_{out} - E^*) \tag{24}$$

$$E_{dref} = E^* + (Q_{ref} - Q_{out}).\left(k_{pq} + \frac{k_{iq}}{s}\right) \tag{25}$$

2.3.3. The Loop Controls Voltage and Current

To ensure that the microgrid meets its voltage and frequency requirements, power conversion is regulated through an internal current control loop. This loop receives its input parameters from an external voltage controller [22].

The current controller, which targets the current across the output reactance of the converter, is designed within the dq rotating coordinate system. This configuration is illustrated in Figure 14. The output from the controller is expressed as a vector signal:

$$u_{di} = v_{td} + \omega L i_q - E_d \tag{26}$$

$$u_{qi} = v_{tq} - \omega L i_d - E_q \tag{27}$$

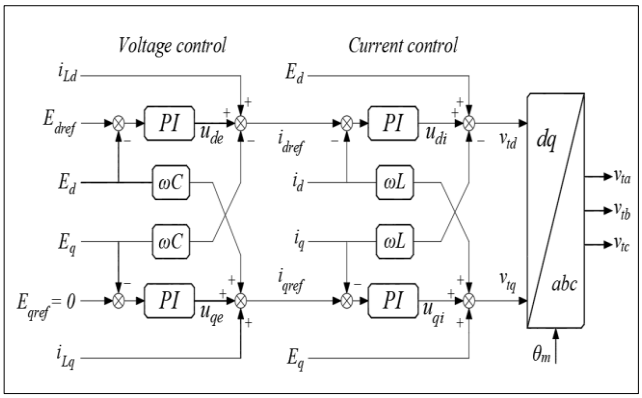

Fig. 14 The loop controls voltage and current

The inner current control loop is presumed to have significantly faster dynamics compared to the outer voltage loop. Therefore, for the voltage loop, constants $i_d \approx i_{dref}$ and $i_q \approx i_{qref}$ can be deemed appropriate.

Controller output signal vector,

$$u_{de} = i_d - i_{Ld} + \omega C E_q \tag{28}$$

$$u_{qe} = i_q - i_{Lq} - \omega C E_d \tag{29}$$

3. Simulation and Results

The effectiveness of the suggested model, which utilizes the VSG controller on the PV-HESS system, is validated using a 6-bus autonomous microgrid model. This microgrid consists of six buses that have been calibrated according to the diagram of the IEEE 6-bus sample grid. The experimental configuration is outlined in Figure 15 and was constructed and simulated using the Matlab/Simulink program. The PV-HESS system parameters are shown in Table 1, whilst the parameters for electrical loads and grid lines are specified separately in Tables 2 and 3, respectively.

The suggested simulation scenario, based on microgrid technology, aims to evaluate the results of incorporating the synchronous generator simulation model into the PV-HESS model framework. This approach showcases the effectiveness of using a voltage source converter to imitate the qualities of a synchronous generator, thus improving system inertia and reducing frequency variations in the microgrid. Figure 16 illustrates the simulation scenario, which encompasses

changeable factors such as fluctuations in solar radiation and changes in grid load capacity. The assessment of the simulation outcomes clearly demonstrates the crucial impact of maintaining a steady compensation, as determined for the microgrid, in the utilization of the synchronous generator simulation model.

Table 1. PV-HESS system parameters

PV Array	Maximum Power	121275 W
	Voltage at MPP	300 V
	Current at MPP	404.25 A
BESS	Nominal Voltage	500 V
	Rate Capacity	1840 Ah
	SOC	90%
	Cut-off Voltage	375 V
	Nominal Discharge Current	800 A
SC	Initial Voltage	540 V
	Rate Capacitance	20 F
VSC	Filter Resistance R_f	3 mΩ
	Filter Inductance L_f	1.5 mH
	Filter Capacitor C_f	2 mF
	Voltage Controller Proportional Gain K_{pv}	15
	Voltage Controller Integral Gain K_{iv}	0.05
	Current Controller Proportional Gain K_{pc}	15
	Current Controller Integral Gain K_{ic}	0.05

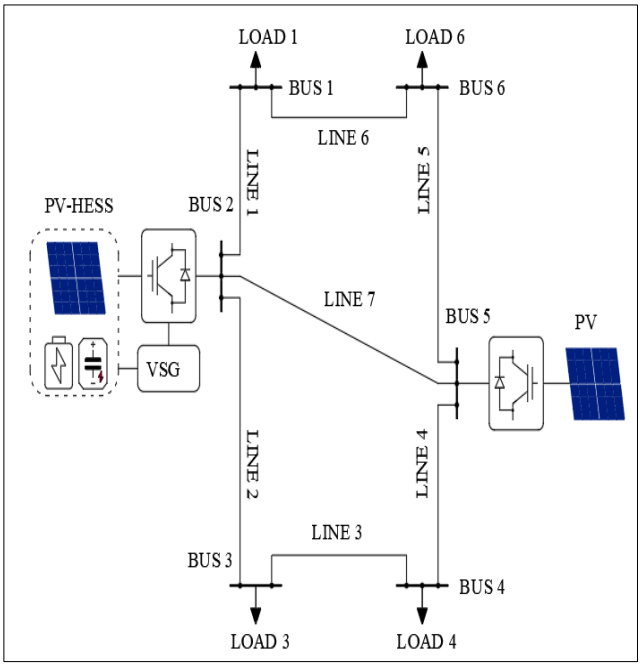

Fig. 15 Autonomous microgrid of 6 bus

Table 2. Load capacity

Load 1	50 + j10 kVA
Load 3	50 + j10 kVA
Load 4	80 + j20 kVA
Load 6	100 + j20 kVA

Table 3. Line impedance

Line 1	0.036 + j0.039 Ω
Line 2	0.072 + j0.108 Ω
Line 3	0.144 + j0.180 Ω
Line 4	0.072 + j0.108 Ω
Line 5	0.144 + j0.180 Ω
Line 6	0.036 + j0.072 Ω
Line 7	0.072 + j0.108 Ω

It is crucial to document the occurrences when agitation becomes evident:

- First fluctuation: Changes in solar radiation conditions occur at 3 seconds and 8 seconds.
- Second fluctuation: Load capacity increases when the entire system is activated, initially operating with load 1 and load 3 at 6 seconds.
- Third fluctuation: Load capacity decreases sharply when loads 3 and 4 are disconnected, as they are no longer required, at 12 seconds.
- Fourth fluctuation: A sudden decrease in the intensity of solar radiation occurs at 15 seconds.
- Fifth fluctuation: The intensity of solar radiation abruptly drops to zero at 20 seconds.

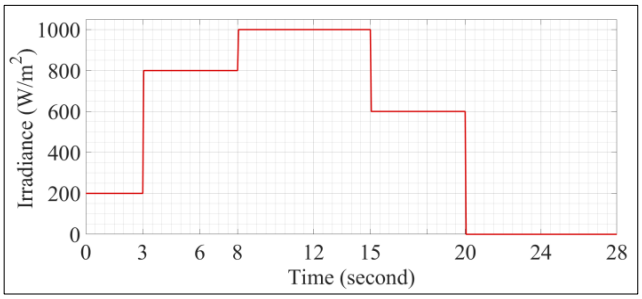

Fig. 16 Solar radiation characteristic

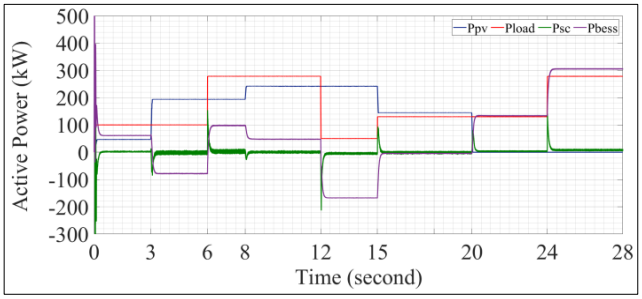

Fig. 17 System power characteristic

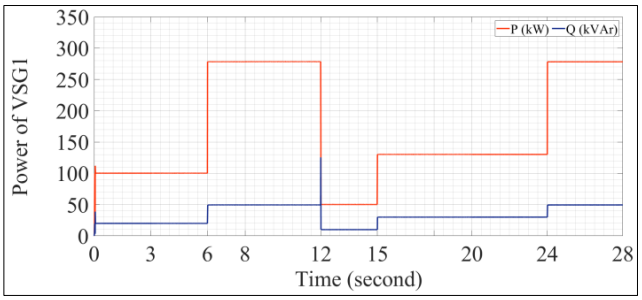

Fig. 18 Active power and reactive power PV – HESS

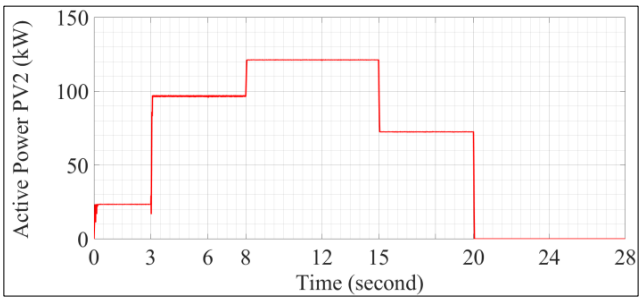

Fig. 19 Active power of PV

Figures 17, 18, and 19 display the simulation findings for the overall power output of the system and its various power source components. Figure 17 presents a comprehensive depiction of the power changes over time for both the source and load systems. Figure 18 illustrates the power dynamics of the PV-HESS hybrid power system. Due to its critical function in grid stabilization, the PV-HESS system experiences fluctuations in both its active and reactive power outputs in reaction to changes in solar radiation and load capacity. The PV-HESS system's intrinsic flexibility allows for quick adjustments to the active and reactive power balance of the grid, ensuring that frequency and voltage levels stay within acceptable limits.

The objective of the simulation process is to assess the performance of the SG simulation model when combined with the PV-HESS model, specifically in relation to grid frequency control. Every stimulation in the simulation is specifically tailored to evaluate the efficacy of this model. Through simulations, we analyze and compare the frequency variations seen in the proposed model with those controlled by the classic droop control method. This comparative analysis is essential to determine the effectiveness of the model in stabilizing grid frequency under different operational scenarios.

Figures 20 and 21 illustrate the simulation findings of grid frequency in response to sudden variations in radiation intensity. The results indicate that the suggested approach consistently offers improved frequency stability in response to rapid changes in radiation levels. Significantly, when the moment of inertia J fluctuates, a higher J value causes less frequency fluctuations, but it also prolongs the time required to reach stability compared to scenarios with a lower J. This demonstrates the crucial importance of the system's inertia in effectively maintaining frequency stability during changing circumstances.

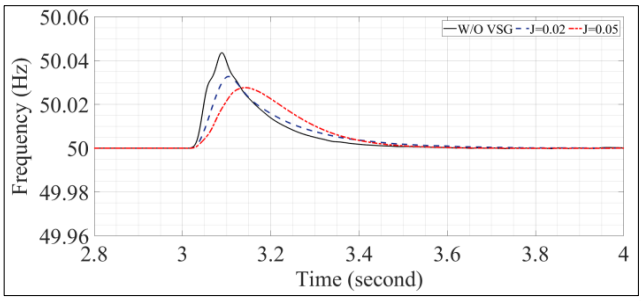

Fig. 20 Frequency at the time of solar radiation changes from 200W/m^2 to 800W/m^2

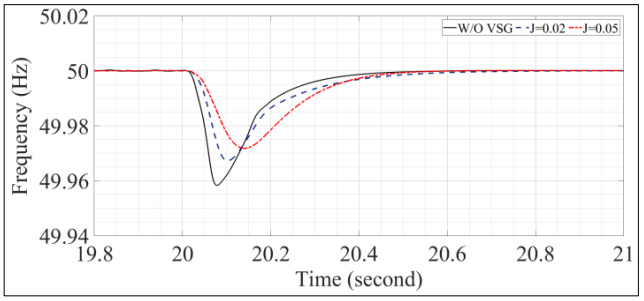

Fig. 21 The frequency of solar radiation changes from 600W/m^2 to 0 W/m^2

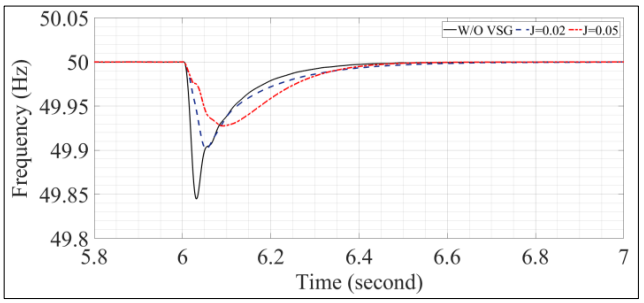

Fig. 22 Frequency at the time of increasing load capacity

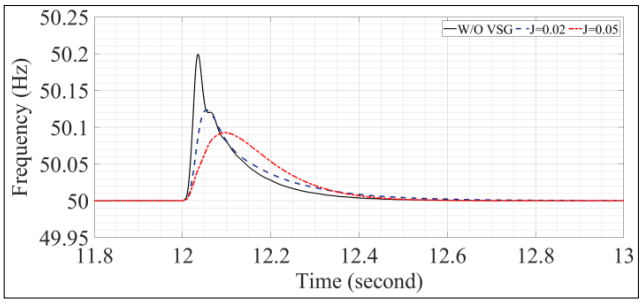

Fig. 23 Frequency at the time of load shedding

Simulation results demonstrate that integrating the PV-HESS system with the SG model yields a much-improved frequency profile compared to typical droop control approaches. This improvement is shown in scenarios with

fluctuating load power, regardless of whether the load is increasing or decreasing. Furthermore, simulations are conducted to explore the relationship between the magnitude of the moment of inertia J and the frequency response. This is achieved by analyzing various values of inertia magnitude. It has been noted that as the value of J increases, the frequency response shows a decrease in overshoot, indicating a more gradual adaptation to changes in load. Nevertheless, an increased value of J also leads to a longer duration required to attain stability. This behavior closely resembles the dynamic response of a synchronous generator when exposed to fluctuating load power excitations. These findings highlight the significance of modifying the moment of inertia in the model to optimize the trade-off between rapid reaction and minimal frequency overshoot. This will improve grid stability when dealing with changing load situations.

Figure 24 illustrates the voltage-current characteristic curve at the DC connection. The PV-HESS system demonstrates minimal voltage fluctuation amplitude and a quicker transient period for stability restoration compared to a standalone PV system. The enhanced performance is credited to the integration of the HESS, which improves the system's ability to respond to changes in voltage. Furthermore, Figures 25 and 26 provide a comprehensive depiction of the State of Charge (SOC) of the HESS, showcasing both the discharge and charging procedures. The graphs illustrate the energy storage dynamics, demonstrating how the HESS effectively controls its charge and discharge cycles to ensure system balance and efficiency. By actively managing the voltage, this process not only stabilizes it but also enhances the operational longevity of the storage components by maximizing their consumption.

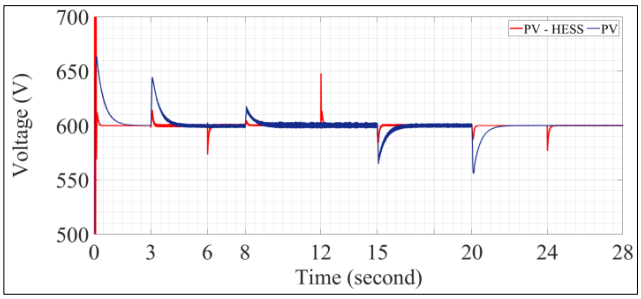

Fig. 24 DC voltage before the power converter

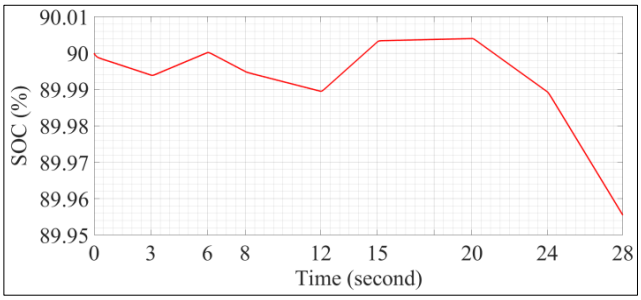

Fig. 25 SOC characteristic curve (%) of the BESS

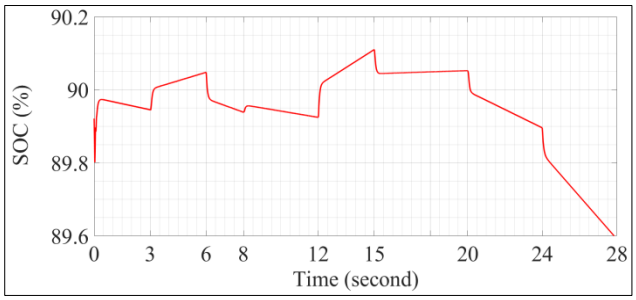

Fig. 26 SOC characteristic curve (%) of supercapacitor

In order to maintain a consistent voltage output in a microgrid, it is necessary to incorporate a voltage source converter and control loops. These control loops are responsible for ensuring that the voltage remains stable under normal operating conditions and adjusts accordingly when there are fluctuations in the system. Implementing a VSG model improves the performance of the VSC controller by allowing it to provide control signals that increase inertia, thereby assisting in the preservation of voltage stability in the microgrid.

The efficacy of these improvements may be demonstrated in the measured voltage and current data at the site of the common coupling node across the given simulated scenarios. The measurements are methodically displayed in Figures 27 and 28. The data demonstrates the ability of the integrated control systems to effectively respond to dynamic changes, showcasing the microgrid's strong voltage regulation capabilities across different operational situations.

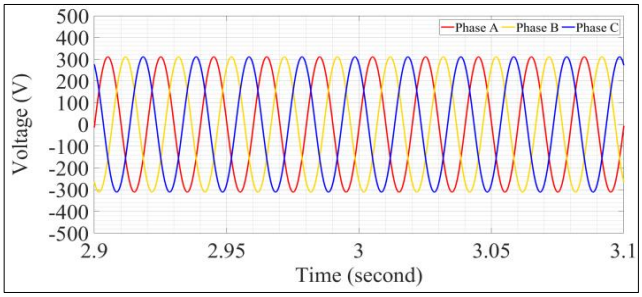

Fig. 27 PCC node voltage when solar radiation changes from 200W/m^2 to 800W/m^2

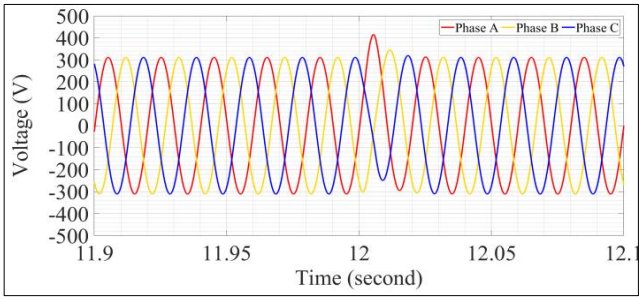

Fig. 28 PCC node voltage at the time of load capacity change

4. Conclusion

The lack of inertia in microgrids has a direct impact on the stability of frequency and voltage, particularly in tiny power grids that function autonomously and rely on distributed sources connected by power converters like PV solar power. While HESS provides support for various PV solar power sources, it is still necessary to address the issue of inertia insufficiency. In order to enhance the performance, it is suggested to implement a VSG controller on the voltage source converter. This will enable the converter to adjust itself according to the specific attributes of a synchronous generator. The authors constructed and tested a simulation model of a synchronous generator based on the PV-HESS system using the Matlab/Simulink tool. The simulation results demonstrate that the suggested model exhibits substantial enhancements in both frequency and voltage profiles, surpassing those achieved by the conventional droop control method. Furthermore, the relationship between the virtual moment of inertia's size, frequency deviation, and the time needed to attain stability following a fluctuation has been examined.

References

[1] Yujia Zhu, and Lili Zhang, "Development of Micro-Grid Control Technique," *2012 Asia-Pacific Power and Energy Engineering Conference*, pp. 1-4, 2012. [CrossRef] [Google Scholar] [Publisher Link]

[2] Weidong Yang, Xia Zhou, and Feng Xue, "Impacts of Large Scale and High Voltage Level Photovoltaic Penetration on the Security and Stability of Power System," *2010 Asia-Pacific Power and Energy Engineering Conference*, pp.1-5, 2010. [CrossRef] [Google Scholar] [Publisher Link]

[3] Thilo Bocklisch, "Hybrid Energy Storage Systems for Renewable Energy Applications," *Energy Procedia*, vol. 73, pp. 103–111, 2015. [CrossRef] [Google Scholar] [Publisher Link]

[4] Reza Hemmati, and Hedayat Saboori, "Emergence of Hybrid Energy Storage Systems in Renewable Energy and Transport Applications - A Review," *Renewable and Sustainable Energy Reviews*, vol. 65, pp. 11-23, 2016. [CrossRef] [Google Scholar] [Publisher Link]

[5] Xingguo Tan, Qingmin Li, and Hui Wang, "Advances and Trends of Energy Storage Technology in Microgrid," *International Journal of Electrical Power & Energy Systems*, vol. 44, no. 1, pp. 179-191, 2013. [CrossRef] [Google Scholar] [Publisher Link]

[6] Ana Fernández-Guillamón et al., "Power Systems with High Renewable Energy Sources: A Review of Inertia and Frequency Control Strategies Over Time," *Renewable and Sustainable Energy Reviews*, vol. 115, 2019. [CrossRef] [Google Scholar] [Publisher Link]

[7] Rongliang Shi, and Xing Zhang, "VSG-based Dynamic Frequency Support Control for Autonomous PV-Diesel Microgrids," *Energies*, vol. 11, no. 7, 2018. [CrossRef] [Google Scholar] [Publisher Link]

[8] Ujjwol Tamrakar et al., "Virtual inertia: Current Trends and Future Directions," *Applied sciences*, vol. 7, no. 7, 2017. [CrossRef] [Google Scholar] [Publisher Link]

[9] Qing-Chang Zhong, and George Weiss, "Synchronverters: Inverters that Mimic Synchronous Generators," *IEEE Transactions on Industrial Electronics*, vol. 58, no. 4, pp. 1259-1267, 2011. [CrossRef] [Google Scholar] [Publisher Link]

[10] K. Sakimoto, Y. Miura, and T. Ise, "Stabilization of a Power System with a Distributed Generator by a Virtual Synchronous Generator Function," *8th International Conference on Power Electronics-ECCE Asia IEEE*, pp. 1498-1505, 2011. [CrossRef] [Google Scholar] [Publisher Link]

[11] Jia Liu et al., "Enhanced Virtual Synchronous Generator Control for Parallel Inverters in Microgrids" *IEEE Transactions on Smart Grid*, vol. 8, no. 5, pp. 2268-2277, 2017. [CrossRef] [Google Scholar] [Publisher Link]

[12] Miguel Torres, and Luiz A. C. Lopes, "Virtual Synchronous Generator: A Control Strategy to Improve Dynamic Frequency Control in Autonomous Power Systems," *Energy and Power Engineering*, vol. 5, no. 2A, pp. 32-38, 2013. [CrossRef] [Google Scholar] [Publisher Link]

[13] Mohd Hanif Othman et al., "Progress in Control and Coordination of Energy Storage System-Based VSG: A Review," *IET Renew. Power Generation*, vol. 14, no. 2, pp. 177-187, 2020. [CrossRef] [Google Scholar] [Publisher Link]

[14] Bhakti Nitve, and Rajani Naik, "Steady-State Analysis of IEEE-6 Bus System Using PSAT Power Toolbox," *International Journal of Engineering Science and Innovative Technology (IJESIT*), vol. 3, no. 3, pp. 2319-5967, 2014. [Google Scholar] [Publisher Link]

[15] Ali Almousawi, and Ammar A. Aldair, "Control Strategy for a PV-BESS-SC Hybrid System in Islanded Microgrid," *Iraqi Journal for Electrical and Electronic Engineering*, vol. 19, no. 1, pp. 1-11, 2023. [CrossRef] [Google Scholar] [Publisher Link]

[16] B. Sai Pranahita et al., "A Study on Modelling and Simulation of Photovoltaic Cells," *International Journal of Research in Engineering and Technology*, vol. 3, no. 11, pp. 2319-1163, 2014. [Google Scholar] [Publisher Link]

[17] Jun Cao et al., "Deep Reinforcement Learning Based Energy Storage Arbitrage With Accurate Lithium-ion Battery Degradation Model," *IEEE Transactions on Smart Grid*, vol. 11, no. 5, pp. 4513-4521, 2020. [CrossRef] [Google Scholar] [Publisher Link]

[18] Mirco Rampazzo et al., "Modelling and Simulation of a Li-ion Energy Storage System: Case Study from the Island of Ventotene in the Tyrrhenian Sea," *Journal of Energy Storage*, vol. 15, pp. 57-68, 2018. [CrossRef] [Google Scholar] [Publisher Link]

[19] Borja Pozo et al., "Supercapacitor Electro-Mathematical and Machine Learning Modelling for Low Power Applications," *Electronics*, vol. 7, no. 4, 2018. [CrossRef] [Google Scholar] [Publisher Link]

[20] Dayan B. Rathnayake et al., "Grid Forming Inverter Modeling, Control, and Applications," *IEEE Access*, vol. 9, pp. 114781-114807, 2021. [CrossRef] [Google Scholar] [Publisher Link]

[21] Roberto Rosso et al., "Grid-Forming Converters: Control Approaches, Grid-Synchronization, and Future Trends - A Review" *IEEE Open Journal of Industry Applications*, vol. 2, pp. 93-109, 2021. [CrossRef] [Google Scholar] [Publisher Link]

[22] Yin Li, and Lingling Fan, "Stability Analysis of Two Parallel Converters with Voltage-Current Droop Control," *IEEE Transactions on Power Delivery*, vol. 32, no. 6. pp. 2389-2397, 2017. [CrossRef] [Google Scholar] [Publisher Link]